Structure characterization and gelling properties of RG-I-enriched pectins extracted from citrus peels using four different methods

Carbohydrate Polymers

Wang, Xueping; Zhao, Chengying; Wang, Jirong; Lu, Xingmiao; Bao, Yuming et al

https://doi.org/10.1016/j.carbpol.2024.122410

Carbohydrate Polymers 342 (2024) 122410

Contents lists available at ScienceDirect

Carbohydrate Polymers

journal homepage: www.elsevier.com/locate/carbpol

Structure characterization and gelling properties of RG-I-enriched pectins extracted from citrus peels using four different methods

Xueping Wang [a,b,1], Chengying Zhao [a,1], Jirong Wang [a], Xingmiao Lu [a], Yuming Bao [c], Deli Zhang [b,*], Jinkai Zheng [a,d,**]

[a] Institute of Food Science and Technology, Chinese Academy of Agricultural Sciences, Beijing 100193, China
[b] Human and Animal Physiology, Wageningen University & Research, 6708 WD Wageningen, the Netherlands
[c] Feed Research Institute, Chinese Academy of Agricultural Sciences, Beijing 100081, China
[d] College of Food Science and Engineering, Qingdao Agricultural University, Qingdao 266109, China

ARTICLE INFO

Keywords:
Citrus
Pectin
RG-I
Chemical structure
Gelling property

ABSTRACT

To facilitate the application of rhamnogalacturonan-I (RG-I)-enriched pectins (RGPs) as novel, healthy, and gelling food additives, this study compared the structural characteristics and gelling properties of RGPs extracted from citrus peel via four methods (alkali: AK, high-temperature/pressure: TP, citric acid: CA, and enzyme-assisted: EA extractions). AK and CA yielded pectins with the highest RG-I proportions (54.8 % and 51.9 %, respectively) by disrupting the homogalacturonan region; TP and EA increased the RG-I proportions by ~10 %. Among the four methods, AK induced the lowest degree of esterification (DE) (6.7 %) and longer side chains that form strong entanglement, contributing to its highest gel hardness. The relatively low DE (18.5 %) of CA RGP facilitated stable gel formation. Notably, its highly branched RG-I region afforded more intramolecular hydrophobic interactions, making a more highly cross-linked gel network of better gel resilience. In contrast, TP induced the highest DE (57 %) and curved molecular chains; it inhibited Ca^{2+} binding, entanglement, and intramolecular hydrophobic interactions, and thus no gel formed. EA RGP was associated with the lowest molecular size, rendering it more difficult for Ca^{2+} to form links, which resulted no gel. These findings offer insights into the relationship among the extraction methods, molecular structures, and gelling properties of RGPs.

1. Introduction

Pectin serves as a cementing substance in plant cell walls, found within the primary cell wall and middle lamella, where it bonds to the cross-linked structure formed by cellulose and hemicellulose. Commercial pectin is predominantly produced from citrus peel (85.5 %) and apple pomace (14.0 %). (Cui et al., 2021). Pectin has emerged as an essential, well-developed ingredient widely used as a gelling agent, emulsifier, thickener, stabilizer, and drug carrier across the food, cosmetics, and pharmaceutical industries. As a complex heteropolysaccharide, pectin primarily comprises three structural domains: ~65 % homogalacturonan (HG), 20–35 % rhamnogalacturonan-I (RG-I), and 2–10 % rhamnogalacturonan-II (RG-II) regions (Moslemi, 2021). The HG region is a smooth linear section composed of galacturonic acid (GalA) residues linked via α (1 → 4) glycosidic bonds. The RG-I and RG-II regions, with abundant and heterogeneous neutral sugar side chains, are referred to as hairy regions. Specifically, the RG-I region exhibits a repeating disaccharide [→2)-α-L-Rhap(1 → 4)-α-D-GalpA-(1→] backbone, with side chains comprising D-galactose (Gal) and L-arabinose (Ara) and four structural variations: arabinan, galactan, arabinogalactan-I (AG-I), and arabinogalactan-II (AG-II) (Naqash et al., 2017).

Compared with commercial pectin, which is mostly HG-dominated, RG-I-enriched pectin (RGP) is characterized by a higher RG-I region content (> 30 %) (Maric et al., 2018). Recent studies have highlighted the remarkable health benefits of RGPs, demonstrating by their abilities to enhance the diversity and relative abundance of beneficial microbiota (Cui, Ren, et al., 2020). The proportion of the RG-I region was positively correlated with anti-inflammatory and immune regulatory effects (Wu et al., 2023), which might protect against cardiovascular diseases

* Corresponding author.
** Corresponding author (Lead contact) at: Institute of Food Science and Technology, Chinese Academy of Agricultural Sciences, Beijing 100193, China.
E-mail address: zhengjinkai@caas.cn (J. Zheng).
[1] Xueping Wang and Chengying Zhao contributed equally to this work.

https://doi.org/10.1016/j.carbpol.2024.122410
Received 10 April 2024; Received in revised form 13 June 2024; Accepted 14 June 2024
Available online 15 June 2024

(Pakhomov & Baugh, 2021). To enhance RGP applications in gel-based healthy products, studies on their gelling properties are urgently needed since they are the primary commercial use of pectin.

Extraction methods influence the structural characteristics of pectin, thus impacting their physicochemical and functional properties, as we previously described (Cui et al., 2021). Various studies have established methods for extracting RGPs, including alkali extraction, organic acid extraction, enzyme-assisted (EA) extraction, and ultrasound/microwave/high-pressure-assisted extraction, along with UV/H_2O_2 oxidation (Niu et al., 2023). Alkali (AK) extraction, the most commonly used method, is efficient for extracting RGPs from numerous materials, including potato (> 70 %), pumpkin (45.4 %), and citrus (64.2 %) (Hou et al., 2022; Khodaei & Karboune, 2013; Zhang et al., 2018; Zhao et al., 2017). In terms of efficiency, high temperature-high pressure extraction (TP) and citric acid (CA) extraction have isolated pectin from red dragon fruit peel with RG-I contents of 72.7 % and 66.6 %, respectively (Zhang & Cai, 2023). Additionally, the environmentally friendly enzyme polygalacturonase can hydrolyze the HG region, achieving RGP extraction (42.3 %) from artichoke (Ferreira-Lazarte et al., 2018). Although there have been studies regarding the yield and increased RG-I proportions, the definitive relationships among extraction methods, chemical structures, and gelling properties of RGPs remain unclear.

In this study, we performed a systematic comparison of the structural characteristics and gelling properties of pectins extracted from citrus peel by four distinct RG-I enrichment methods. The study revealed differences in the RG-I proportion, primary structures, and spatial conformations of pectin samples extracted via AK, TP, CA, and EA extraction. Furthermore, we explored their gelling properties, extensively characterizing the relationships among extraction methods, chemical structures, and gelling properties. Our findings provide insights for the efficient preparation and industrial applications of RGPs.

2. Materials and methods

2.1. Materials and reagents

Air-dried peels of *Citrus reticulata* 'Chachiensis' were purchased from a local company in Jiangmen, Guangzhou, China, and grounded into the 40-mesh powder with a grinder (FSJ-A03E1, Xiaoxiong, China). The enzyme *endo*-Polygalacturonase (Endo-PGALPC, E.C.3.2.1.15) from *Pectobacterium carotovorum* (540 units/mg) was purchased from Megazyme Co., Ltd. (Bray, Ireland). Dialysis bags (10 and 3.5 kDa) were purchased from Solarbio Life Science Co., Ltd. (Beijing, China). Monosaccharide standards, including galacturonic acid (GalA), rhamnose (Rha), arabinose (Ara), galactose (Gal), glucose (Glc), xylose (Xyl), and fucose (Fuc) were obtained from Sigma-Aldrich (Shanghai, China). Trifluoroacetic acid and 95 % ethanol were obtained from Aladdin Biochemical Technology Co., Ltd. (Shanghai, China). All other chemicals including hydrochloric acid (HCl), sodium hydroxide (NaOH), citric acid (CA), potassium bromide (KBr), deuterium oxide (D_2O), and calcium chloride dihydrate ($CaCl_2$) were of analytical grade and purchased from Macklin Biochemical Technology Co., Ltd. (Shanghai, China).

2.2. Extraction methods for RGPs

RGPs were extracted using previously established methods with minor modifications (Khodaei & Karboune, 2013; Niu et al., 2023; Zhao et al., 2017), and the conventional hot-acid (HA) method served as the control group (Cui, Zhao, et al., 2020). For all groups, peel powder was suspended in deionized water at a ratio of 1:40 w/v, and these mixtures were used for further extraction. In HA and AK group, the pH of the mixture was adjusted to 2.0 and 10.5 with HCl and NaOH, then stirred in a water bath at 80 °C and 50 °C, respectively. For TP extraction, the mixture was placed in a high-pressure steam apparatus (LDZX-50FBS, Shenan, China) under 0.2 MPa pressure for a holding time of 15 min at 115 °C to yield RGP. In CA group, 0.8 % (w/v) CA was added to the mixture, and then stirred in the water bath at 65 °C for 80 min (Zhang & Cai, 2023). EA RGP was prepared by enzyme treatment on the HA pectin solution (1:30, w/v). The pH of the solution was adjusted to 4.5, then Endo-PGALPC (40 units/g) was added (Khodaei & Karboune, 2013). After incubated for 30 min at 40 °C, the solution was immersed in boiling water for 5 min to inactivate the enzyme. In all groups, the pH was adjusted to 6.2 and centrifugated to remove insoluble matter. The supernatants were concentrated to half their volume and precipitated by adding 95 % ethanol (1:3, v/v). After the precipitates had been stored at 4 °C overnight, they were washed twice with 95 % ethanol and dialyzed for 72 h (10 kDa cutoff for HA, AK, TP, and CA group; 3.5 kDa cutoff for EA group). All dialyzed solutions were then frozen and lyophilized for 72 h to obtain dry RGPs. Each extraction process was performed in triplicate. Pectin yield was calculated using the following equation:

$$\text{Pectin yield}\ (\%) = \frac{\text{wt}}{\text{w0}} \times 100\% \quad (1)$$

where wt and w0 represent the dry weights of the extracted pectins and citrus peels, respectively.

2.3. Primary structure determination

2.3.1. Molar mass

The molar masses of RGPs were determined using a combination of multi-angle laser light scattering and high-performance size exclusion chromatography (SEC) (L2130; Hitachi, Tokyo, Japan), as reported by Wang et al. (2023). The weight-average molar mass (Mw) and number-average molar mass (Mn) of the pectins were analyzed and processed using ASTRA 5.3.4 software (Wyatt Technology, Santa Barbara, CA, USA).

2.3.2. Monosaccharide composition

The monosaccharide compositions of RGPs were determined by high-performance anion-exchange chromatography (ICS-3000; Dionex, Sunnyvale, CA, USA), with pretreatment as described in our previous study (Cui, Zhao, et al., 2020). All dilutions and monosaccharide standard mixtures (0.01–5 mg/L of GalA, Rha, Ara, Gal, Glc, Xyl, and Fuc) were filtered through 0.22-μm membrane filters before analysis. The flow rate of the eluent, a sodium hydroxide aqueous solution (250 mmol/L) and sodium acetate aqueous solution (1 mol/L), was 0.5 mL/min.

2.3.3. Fourier transform infrared (FT-IR) spectroscopy

FT-IR spectra were collected in absorbance mode from 4000 to 400 cm^{-1} using a TENSOR 27 FT-IR spectrometer (Bruker, Karlsruhe, Germany). The dried sample was mixed with KBr powder at a ratio of 1:50 and compressed into 1 mm thick tablets. The degree of esterification (DE) of RGPs was calculated using the following equation (Pappas et al., 2004):

$$\text{DE}\ (\%) = 124.7 \times \frac{\text{A1753}}{\text{A1753} + \text{A1641}} + 2.2013 \quad (2)$$

where A_{1753} and A_{1641} represent the peak areas of absorption at 1753 and 1641 cm^{-1}, respectively.

2.4. Nuclear magnetic resonance (NMR) spectroscopy

The chemical structures of RGPs were also analyzed by NMR spectroscopy as described in previous study (Lu et al., 2024). ^1H and ^{13}C NMR spectra of RGPs were determined using AVANCE III HD 600 MHz NMR spectrometer (Bruker, Germany). Chemical shifts were expressed in δ (ppm), using the residual solvent signal of D_2O as reference. All spectra were manually baseline-corrected and analyzed with MestReNova 12.0.0 software (MestreLab Research, Santiago de Compostela,

Table 1
Primary structural information of RGPs extracted by different methods.

	HA pectin	AK RGP	TP RGP	EA RGP	CA RGP
Yield (%)	13.7 ± 0.5^{b}	2.8 ± 0.4^{e}	6.3 ± 0.5^{d}	8.1 ± 0.5^{c}	15.5 ± 1.5^{a}
Mn (10^5 g/mol)	0.7 ± 0.0^{a}	0.6 ± 0.0^{b}	0.5 ± 0.0^{c}	0.1 ± 0.0^{d}	0.5 ± 0.0^{c}
Mw (10^5 g/mol)	1.1 ± 0.0^{a}	0.7 ± 0.0^{b}	0.7 ± 0.0^{c}	0.2 ± 0.0^{e}	0.5 ± 0.0^{d}
Mw/Mn	1.6 ± 0.0^{a}	1.3 ± 0.2^{b}	1.3 ± 0.1^{b}	1.5 ± 0.2^{a}	1.1 ± 0.1^{b}
GalA (mol%)	73.6 ± 4.2^{a}	34.9 ± 3.3^{d}	60.8 ± 2.4^{b}	63.1 ± 3.8^{b}	47.0 ± 2.4^{c}
Rha (mol%)	1.8 ± 0.3^{c}	3.4 ± 0.5^{b}	2.4 ± 0.4^{c}	2.6 ± 0.5^{bc}	5.5 ± 0.1^{a}
Ara (mol%)	12.5 ± 2.3^{c}	29.4 ± 1.6^{a}	20.4 ± 1.7^{b}	18.4 ± 0.2^{b}	29.6 ± 2.5^{a}
Gal (mol%)	8.3 ± 0.3^{b}	18.6 ± 0.4^{a}	9.8 ± 2.7^{b}	10.8 ± 0.8^{b}	11.3 ± 0.3^{b}
Glu (mol%)	2.3 ± 1.6^{a}	6.1 ± 0.1^{a}	4.4 ± 1.9^{a}	3.5 ± 2.7^{a}	4.5 ± 0.4^{a}
Xyl (mol%)	0.8 ± 0.3^{b}	5.9 ± 1.0^{a}	1.5 ± 0.2^{b}	1.0 ± 0.4^{b}	1.4 ± 0.5^{b}
Fuc (mol%)	0.2 ± 0.2^{b}	0.9 ± 0.3^{a}	0.3 ± 0.1^{b}	0.2 ± 0.1^{b}	0.3 ± 0.1^{b}
HG (%)	71.8 ± 4.5^{a}	31.5 ± 3.8^{d}	58.4 ± 2.0^{b}	60.5 ± 3.3^{b}	41.5 ± 2.5^{c}
RG-I (%)	24.4 ± 2.7^{c}	54.8 ± 3.0^{a}	35.1 ± 0.2^{b}	34.4 ± 0.1^{b}	51.9 ± 2.5^{a}
(Ara + Gal)/Rha	11.9 ± 0.9^{ab}	14.3 ± 1.5^{a}	12.6 ± 2.4^{a}	11.6 ± 2.7^{ab}	7.4 ± 0.2^{c}
DE (%)	52.0 ± 0.1^{b}	6.7 ± 0.0^{e}	57.0 ± 0.2^{a}	33.4 ± 0.7^{c}	18.5 ± 0.0^{d}

* Different letters denote significantly different in the row ($p < 0.05$).
** HG (%) = GalA (%) - Rha (%).
*** RG-I (%) = 2 × Rha (%) + Ara (%) + Gal (%).

Spain).

2.5. Atomic force microscopy (AFM)

The nanostructure and branches of RGPs were characterized by AFM (NX-10, Park Scientific Instruments, Suwon, South Korea) using non-contact mode as preciously described (Cui, Zhao, et al., 2020). The scanning area was set at 2.5 × 2.5 μm and 500 × 500 nm with a scanning resolution of 256 × 256 points. AFM images were processed and analyzed with XEI software (Park Systems, Suwon, South Korea).

2.6. Small-angle X-ray scattering (SAXS) analysis

SAXS was detected on Anton Paar SAXSpoint 5.0 instrument at room temperature according to our previously reported method (Cui, Zhao, et al., 2020). The data was analyzed with GIFT software (Anton Paar, Graz, Austria). The distance distribution function P (r) in real space was obtained by indirect Fourier transform of the scattering curve I (q) in reciprocal space. The radius of gyration (Rg) and cross-sectional radius (Rc) were measured by Guinier analysis and cross-sectional Guinier analysis, whose values were estimated by Eqs. (3) and (4) respectively.

$$I(q) \cong I(0)exp\left(-\frac{1}{3}q^2Rg^2\right) \quad (3)$$

$$qI(q) \cong I(0)exp\left(-\frac{1}{2}q^2Rc^2\right) \quad (4)$$

I (0)-the intensity at zero angle; $q = 4\pi\sin\theta/\lambda$; θ-scattering angle; λ-wavelength. All data were background subtracted from the scattering of solvents.

2.7. Gelling properties

2.7.1. Calcium-induced gel formation

Calcium-induced pectin gels were prepared to compare the gelling properties of RGPs. When preparing gels, 5 mL amounts of pectin solutions (2 % w/v) and 0.5 mL amounts of calcium chloride solution (0.3 mol/L) were combined and mixed well. The gels were left to stand for 12 h at 4 °C before further testing.

2.7.2. Texture test

The texture of RGP gels was analyzed using a texture analyzer (TA-XT2i, Stable Micro Systems Ltd., Surrey, UK). The gel specimens used in the textural tests were 27 mm in diameter and 18 mm in height. RGP gels were placed on a fixed bottom plate under the probe (P/0.5 probe, 25 mm diameter) until deformation reached 40 %. The speed of pre-test, test, and post-test were set to 1.0, 0.5, and 1.0 mm/s respectively. The trigger force was 1 g (0.0098 N) and the time between two loadings was 5 s (Wang et al., 2023). Gel hardness, gumminess, chewiness, and resilience were calculated with Texture Expert 1.22 software (Stable Micro Systems Ltd., Surrey, UK).

2.7.3. Rheological measurement

The rheological properties of RGP gels were measured at room temperature using a HAAKE RheoStress 6000 rheometer (Thermo Scientific, Waltham, MA, USA). Briefly, 2.3 g RGP gel was placed on the 40 mm parallel plate for the stress sweep test at 1 Hz to determine the linear viscoelastic region of gel samples. The gap in the parallel plates during rheological measurements was 1 mm. With the deformation (less than the maximum value of the linear viscoelastic range) of 0.1 %, the changes in storage modulus (G′) and loss modulus (G″) of RGP gels were monitored via angular frequency sweep in the range of 0.1–10 Hz.

2.7.4. Scanning electron microscopy (SEM)

The surface morphologies of RGPs and freeze-dried RGP gels were observed with SEM (SU8010; Hitachi, Ibaraki, Japan). The RGPs and freeze-dried gel cross-sections were fixed onto the conductive adhesive of the sample stage with a gold powder layer coated under vacuum. The SEM images of the samples were observed at different acceleration voltages consisting of multiples of 10 kV.

2.8. Statistical analysis

All experiments were performed in triplicate and data were expressed as means ± standard deviation (SD). Significant differences between different groups were performed using one-way analysis of variance (ANOVA) and Duncan's tests by SPSS Software 26.0 (IBM, Chicago, IL, USA), and $p < 0.05$ was taken to indicate statistical significance. Origin 2021 software was used for graphic presentation.

3. Results and discussion

3.1. Yield and RG-I proportions

We first investigated the yield and RG-I proportion of pectins extracted by various methods (Table 1). The yields were 13.7 %, 2.8 %, 6.3 %, 8.1 %, and 15.5 % for HA, AK, TP, EA, and CA, respectively, demonstrating significant differences among the methods. Both inorganic and organic acid extraction methods had higher yields than other methods; AK produced the lowest yield. Compared with HA pectin, all

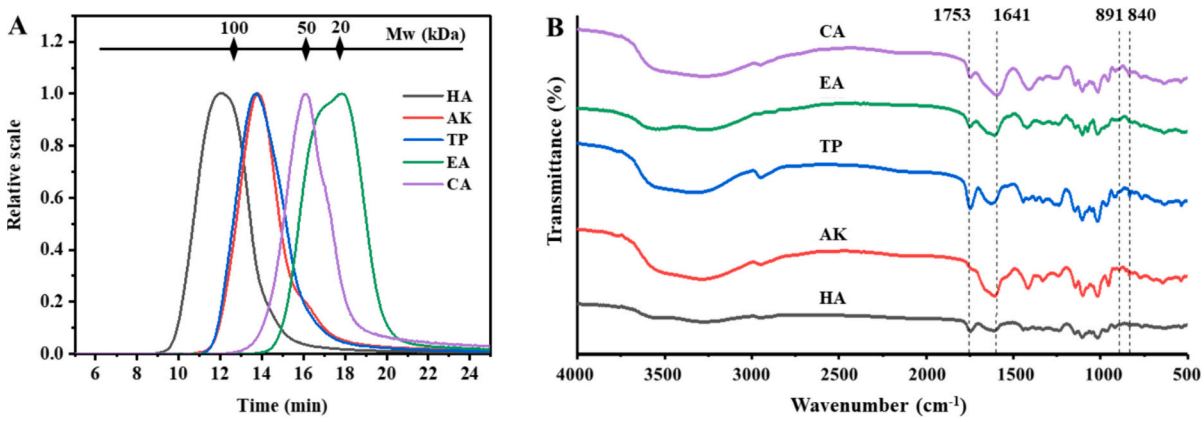

Fig. 1. SEC (A) and FT-IR (B) spectra of RGPs extracted by different methods.

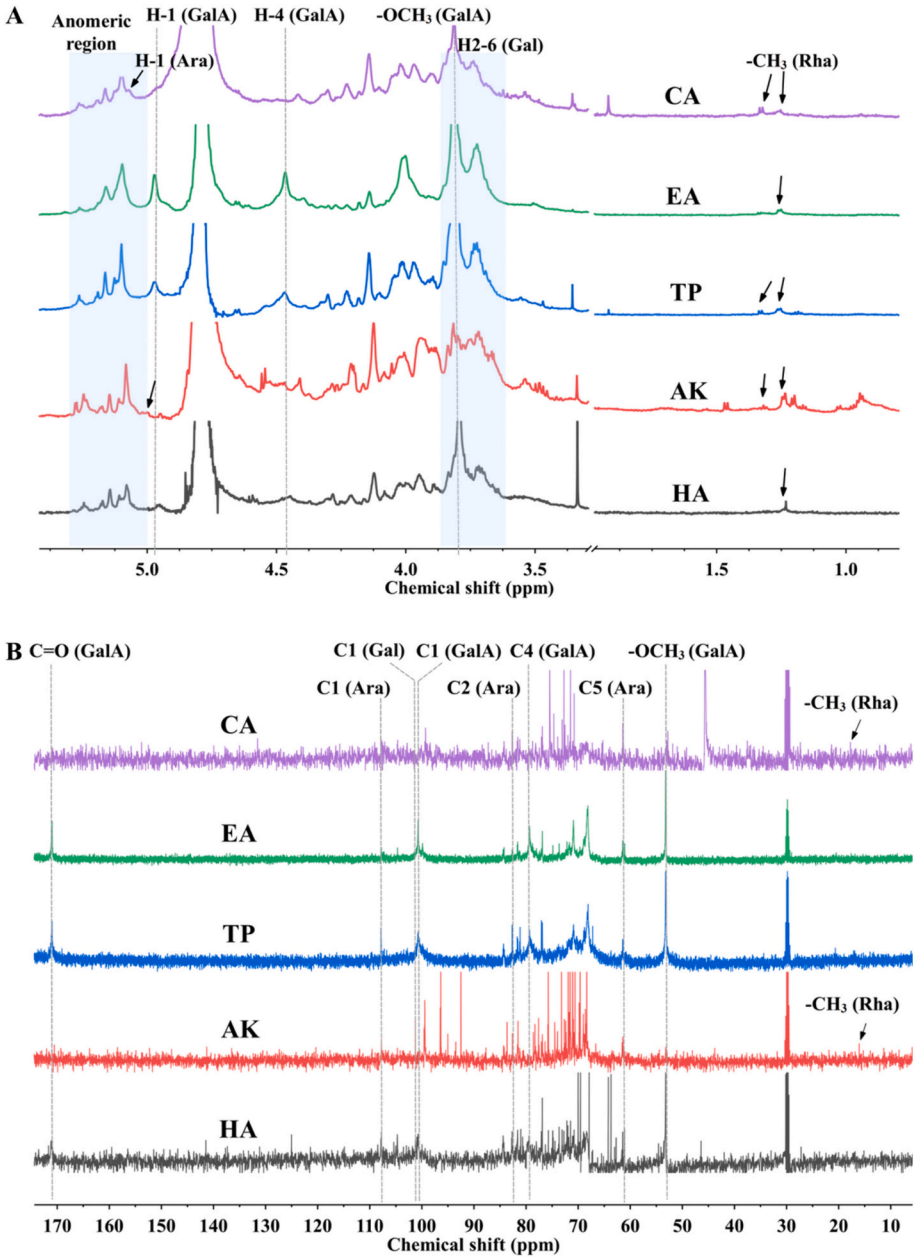

Fig. 2. ^{1}H (A) and ^{13}C (B) NMR spectra of RGPs extracted by different methods.

pectins extracted by RG-I enriching methods displayed a higher proportion of the RG-I region, indicating the efficacy of the four methods used to obtain RGPs in this study. Specifically, as illustrated in Table 1, AK and CA achieved the highest RG-I proportions (54.8 % and 51.9 %). The RG-I proportions of TP and EA pectins were ~ 10 % greater than that of HA pectin. Both methods are considered environmentally friendly; however, they might exhibit lower effectiveness with higher costs during further application in the citrus pectin production industry. CA extraction, with its high yield and RG-I proportion, was considered a suitable method for industrialization.

3.2. Primary structures of RGPs extracted by different methods

3.2.1. Molar mass

As shown in Fig. 1A, the molar weight distribution peaks (the signals from the light scattering detector) were broad for all samples. The values in Table 1 are the average molecular weights. Compared with HA pectin (Mw 1.1 × 10^5 g/mol, Mn 0.7 × 10^5 g/mol), the molar mass of RGPs decreased to varying extents, suggesting that all enrichment methods could disrupt the structure of the pectin HG main chain while preserving more RG-I regions; these factors could lead to a reduction in molar mass. Notably, the molar mass of EA RGP (Mw 0.2 × 10^5 g/mol, Mn 0.1 × 10^5 g/mol) was significantly lower than that of other RGPs. Endo-PGALPC was able to hydrolyze the α (1 → 4) glycosidic bonds between GalA residues, segmenting the pectin chain. Then, shorter chains of HG sections (< 3.5 kDa) were dialyzed out, resulting in molecules with an enriched RG-I region.

3.2.2. Monosaccharide composition

RGPs extracted by various methods showed diverse monosaccharide compositions, indicating that the extraction method had a substantial impact on their primary structures. Compared with HA pectin, all RGPs showed a reduced proportion of GalA and an increased proportion of Ara. AK showed the lowest proportion of GalA (34.9 %) due to the degradation of its HG chain through the β-elimination reaction under alkaline conditions. Significant increases in Ara (29.4 %) and Gal (18.6 %) were observed in AK, suggesting that side chains in the RG-I region were effectively released from the cell wall and preserved under low-temperature alkaline conditions. AK RGP had the highest value of the ratio (Ara + Gal)/Rha (14.3); it likely exhibited an RG-I-enriched structure with long side chains. Unlike other RG-I-enriched samples, the proportions of Gal and Rha in TP and EA did not significantly differ from HA pectin, leading to a minor increasement of RG-I proportion. This minimal increasement could be attributed to the inefficient or incomplete release of side chains in TP, as well as the potential hydrolysis effect of Endo-PGALPC on the linkage of Gal and Rha during EA extraction. In CA, the proportion of GalA (47.0 %) also sharply decreased, whereas Rha and Ara substantially increased to 5.5 % and 29.6 %, respectively. Considering that Rha is regarded as the branch point of the hairy region, CA RGP exhibited a highly branched primary structure. These findings suggest that CA can degrade the main chain structure of the HG region while preserving side chains on the RG-I region (Zhang & Cai, 2023).

3.2.3. FT-IR spectroscopy and DE

The FT-IR spectra in Fig. 1B display characteristic absorption peaks of RGPs. The distinct absorption peaks of pectin at around 3427, 2935, and 1148 cm^{-1} resulted from the inter- and intramolecular hydrogen stretching of O—H, C—H, CH2, CH3, and C-O-C in glycosidic compounds (Yu et al., 2021). A similar pattern of absorption peaks, observed among samples (except for EA) from 1200 to 800 cm^{-1}, belongs to the fingerprint region of carbohydrates. This region provides information about the major chemical groups in polysaccharides (Spinei & Oroian, 2022). The peaks in the range of 920–950 cm^{-1} indicated the presence of furanose and pyranose rings (Hu et al., 2021). The difference in EA might be related to the degradation of both the pectin main chain and neutral side chains during enzymatic treatment, resulting in an atypical pectin FT-IR spectrum. The weak band near 891 cm^{-1} indicated the existence of β-configurations (Li et al., 2021), with Gal units connected to the RG-I region through β (1 → 2) and (1 → 4) linkages (Chandel et al., 2022). The stronger absorption in AK suggested a superior protection effect of Gal side chains during alkali extraction. The weak band around 840 cm^{-1} corresponded to arabinose in the pectin structure (Spinei & Oroian, 2023); the stronger absorption in CA indicated preservation of Ara side chains during the extraction process. In contrast, EA and HA exhibited weaker absorption in this region, indicating the loss of arabinose during extraction.

The DE is a crucial factor that affects the gelling properties of pectin. As shown in Table 1, the DEs of RGPs (HA, AK, TP, EA, and CA) were 52.0 %, 6.7 %, 57.0 %, 33.4 %, and 18.5 %, respectively. The demethylation of polygalacturonic chains under alkaline conditions resulted in the lowest DE in AK. TP exhibited a higher DE than HA pectin, possibly related to the activated methyl esterification reaction in the acidic condition of citrus peel solution under high temperature and high pressure. The DE in EA significantly decreased, suggesting that hydrolysis of the HG main chain during enzymatic treatment led to the shedding of methyl groups. Intriguingly, although the CA extraction was also conducted under acidic conditions, its DE was much lower than that of HA pectin, indicating that the CA-induced disruption of the main chain structure of the HG region also led to the shedding of methyl groups.

3.3. Fine structures of RGPs extracted by different methods

3.3.1. ^{1}H NMR spectroscopy

^{1}H NMR spectra in Fig. 2A provided detailed molecular structural information about RGPs. The proton signals of H-1, H-2, H-3, H-4, and H-5 in GalA were observed at 4.96, 3.61, 3.90, 4.47, and 4.63 ppm, respectively (Zheng et al., 2020). Compared with HA pectin, AK and CA exhibited decreased signals at H-1 and H-4, whereas TP showed no significant changes. These results suggested that AK and CA extraction led to degradation of the GalA chain structure. Conversely, TP preserved the GalA main chain structure; this result differed from the reported destruction of the structure of the HG region (Zhang & Cai, 2023), possibly due to variations in raw material. The peak around 3.82 ppm, attributed to methyl-esterified GalA units (Cheng & Neiss, 2012), was consistent with the DE values presented in Table 1. Signals at 1.27 and 1.36 ppm, originating from methyl groups of unbranched α (1 → 2)-linked and branched α (1 → 2)- and α (1 → 4)-linked rhamnose (Alba et al., 2015), were observed. The peak at 1.27 ppm appeared in all samples, but only AK, TP, and CA RGPs exhibited a significant peak at 1.36 ppm; CA demonstrated the strongest signal, indicating better preservation of branched Rha during CA extraction. Additionally, signals from 3.61 to 3.84 ppm, attributed to H-2, H-3, H-4, H-5, and H-6 of Gal (Zhou et al., 2018), were more complex and intensive in AK than in other RGPs, corresponding to the highest content of Gal in AK; these results confirmed the preservation of Gal during AK extraction. In the anomeric region, signals ranging from 5.0 to 5.3 ppm represented H-1 in various anomeric configurations (α/β) of Ara (Zhang et al., 2018). Specifically, the signals at ~5.00 ppm and 5.04 ppm referred to H1 in unbranched α (1 → 5)-linked and branched α (1 → 3)- and α (1 → 5)-linked arabinose, respectively (Zheng et al., 2020). Although both possessed a high concentration of Ara, the former signal was observed only in AK, whereas the latter was exclusive to CA. The distribution of Ara signals in the spectra highlighted differences in side chain structure, indicating that AK preserved longer Ara chains, whereas CA tended to maintain a more branched structure with shorter side chains. Compared with other RGPs, the ^{1}H NMR spectra of EA RGP in the abovementioned ranges were much simpler and contained fewer signals, emphasizing the destructive effect of the enzyme on Gal and Ara linkages.

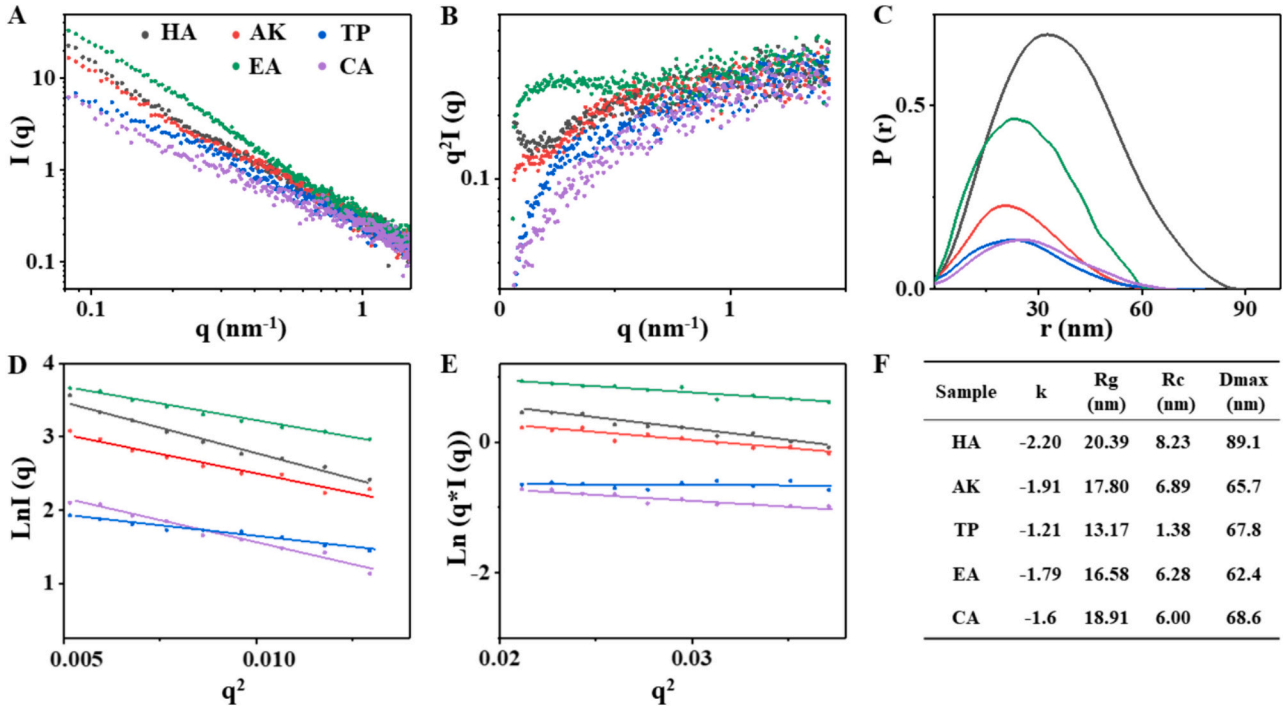

Sample	k	Rg (nm)	Rc (nm)	Dmax (nm)
HA	-2.20	20.39	8.23	89.1
AK	-1.91	17.80	6.89	65.7
TP	-1.21	13.17	1.38	67.8
EA	-1.79	16.58	6.28	62.4
CA	-1.6	18.91	6.00	68.6

Fig. 3. SAXS analysis of RGPs extracted by different methods. (A) Typical SAXS intensity plots of different pectin solutions at a concentration of 1 % (w/v). (B) Typical Kratky plots of the SAXS scattering profiles. (C) Normalized P(r) curves of SAXS scattering profiles. (D) Guinier Rg plots of the SAXS profile. (E) Cross-sectional Guinier Rc plots of the SAXS profiles. (F) Summary table of dimensional information.

3.3.2. ^{13}C NMR spectroscopy

^{13}C NMR spectra of RGPs are presented in Fig. 2B. The signals around 172.0 and 54.1 ppm originated from the carboxyl groups (C=O) and the methyl groups bound to carboxyl groups (-OCH3) of GalA, respectively (Alba et al., 2015). In the spectra of AK and CA RGPs, the signal at 172.0 ppm was scarcely observable, and the signal at 54.1 ppm was substantially weaker than in other samples, consistent with the contents of GalA and DE. The C-1, C-2, C-3, C-4, C-5, and C-6 carbon atoms in GalA corresponded to signals at 100.8, 68.9, 70.7, 79.5, 73.7, and 173.5 ppm, respectively (Ho et al., 2023). Noticeable decreases in the signals of GalA C-1 and C-4 in both AK and CA indicated degradation of the α (1 → 4) linkage in the HG region. The signal at 17–18 ppm in the high-field region was associated with the methyl groups in Rha (Alba et al., 2015). Among all RGPs, only AK and CA exhibited weak signals in this region, suggesting a branched structure with Rha junctions. Therefore, it can be inferred that AK and CA enriched the RG-I proportion by degrading the GalA main chain while preserving more Rha. The signal of Gal C-1 was only observed in the spectra of AK RGP at around 101.3 ppm (Ho et al., 2023), implying that the Gal side chain was protected and enriched during AK extraction. Signals around 62.0, 82.0, and 108.0 ppm corresponded to C-5, C-2, and C-1 in Ara (Lin et al., 2016; Sun et al., 2015); these signals were distinctly present in CA, indicating better preservation of Ara structure during CA extraction. In contrast, these signals were weakened or absent in the spectra of TP and EA, suggesting ineffective release and hydrolysis of side chains during their extraction processes.

3.4. Conformational analysis of RGPs extracted by different methods

3.4.1. SAXS analysis

SAXS was used to analyze the conformations of RGPs in solution. The slope (k) in the low-q zone of intensity plots (Fig. 3A) indicates the overall stereo shape of samples (k = 0 for sphere, k = −1 for column, and k = −2 for plate) (Chivero et al., 2014; Li et al., 2016). The k values for HA pectin, AK, and EA RGP were − 2.2, −1.91, and − 1.79, respectively, suggesting a plate-like conformation. TP (−1.21) and CA (−1.60) showed smaller k values than the others, suggesting a columnar shape with a large cross-sectional radius. The Kratky plot (Fig. 3B) was used to distinguish the conformations of RGPs (Yang et al., 2018). AK RGP's Kratky plot showed a monotonic increase until reaching a plateau at high q, indicative of a Gaussian chain structure (Saffer et al., 2014). The Kratky plots of TP and CA became linearized at high q, suggesting a rod-like structure. EA RGP displayed a peak within the recorded q-regime, characteristic of a three-dimensional mass fractal structure (Hermansson et al., 2016). The pair distance distribution function P(r) revealed particle size information about macromolecules through the model-independent Dmax. As shown in Fig. 3C, EA RGP had the smallest Dmax (62.4 nm), whereas reductions of >20 nm compared with HA pectin (89.1 nm) were observed in the other samples, likely because of HG main chain degradation. The Dmax of AK RGP (65.7 nm) was smaller than the values for TP (67.8 nm) and CA (68.6 nm), due to more extensive main chain degradation under alkaline conditions; this low value led to a compact conformation in AK.

Guinier analysis [ln I(q) vs q^2] (Fig. 3D) and cross-sectional Guinier plots [ln (qI(q)) vs q^2] (Fig. 3E) at low q-values determined the Rg and Rc (Cui, Zhao, et al., 2020). Rg represents the average distance of a polymer from its center of mass, indicating the association state, whereas Rc represents the radius of molecular cross-section, offering insights into molecular bending. As summarized in Fig. 3F, all RGPs exhibited smaller Rg and Rc compared with HA pectin (Rg 20.39 nm, Rc 8.23 nm), indicating tighter spatial conformations associated with increased RG-I proportions. TP RGP had the smallest Rg (13.17 nm) and Rc (1.38 nm), consistent with its columnar shape. After enzyme treatment of HA pectin with Endo-PGALPC, EA RGP showed reduced Rg (16.58 nm) and Rc (6.28 nm), indicating the spatial size reduction was correlated with HG region degradation. Although AK and CA RGP shared similar RG-I proportions, their conformations differed due to distinct molecular structures. AK extraction preserved longer side chains, leading to a larger Rc (6.89 nm) and smaller Rg (17.80 nm) because of local chain bending from counterion condensation.

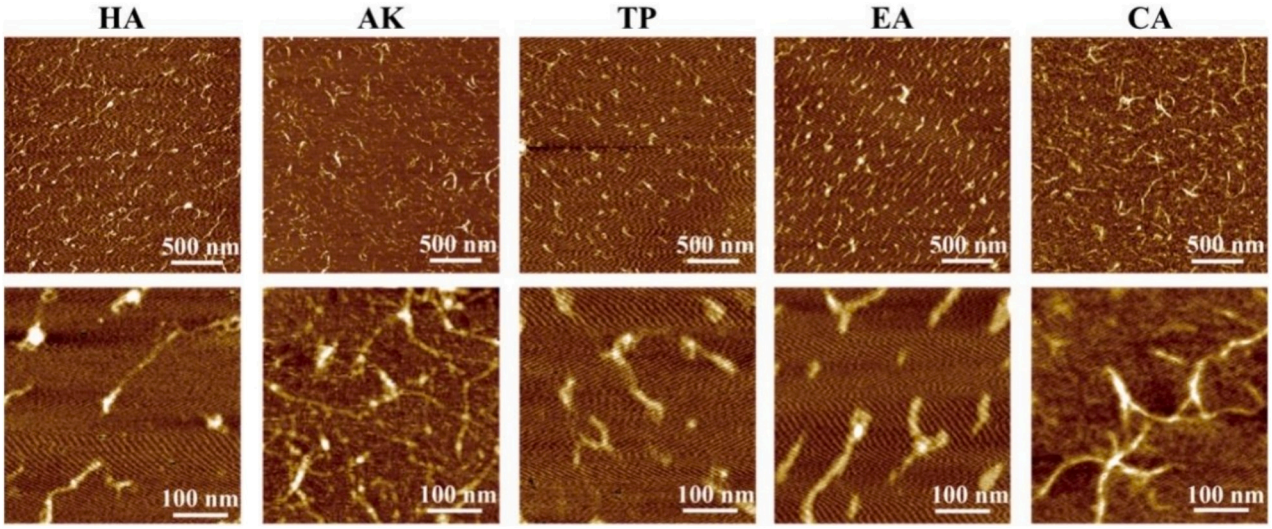

Fig. 4. AFM images of RGPs extracted by different methods.

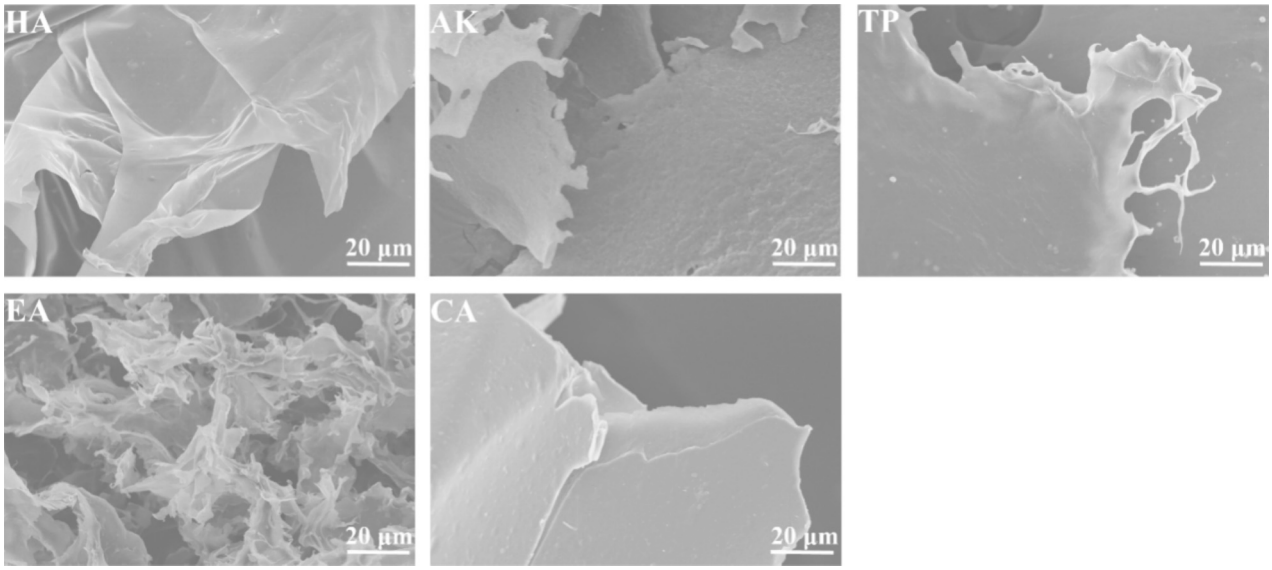

Fig. 5. SEM images (1000× magnification) of RGPs extracted by different methods.

Conversely, CA extraction retained more branch points with relatively short side chains, resulting in a smaller Rc (6.0 nm) and larger Rg (18.91 nm).

3.4.2. *Microscopic observation*

AFM was used to further examine the nanostructures of RGPs. As shown in Fig. 4, the molecular nanostructures of the samples varied according to the extraction method. HA pectin presented a long linear filamentous structure (Cui, Zhao, et al., 2020). AK and CA RGPs exhibited a highly branched molecular morphology with a complex cross-linked network structure; molecules appeared closer and more tightly entangled in CA. TP molecules demonstrated a curved morphology, where the ends of their molecular chains were bent and folded irregularly because of the high pressure during extraction that applied deforming forces on the flexible endpoints. Consistent with changes in molar mass and monosaccharide composition, the molecular chain of EA RGP was segmented into smaller fractions, generating more branched fractions after enzymatic treatment and dialysis.

SEM was used to visualize the surface morphologies of RGPs (Fig. 5). HA pectin displayed a thin and lamellar structure, whereas AK appeared rough and loose, possibly due to the presence of long-tangled side chains. TP exhibited a smooth surface with a texture that appeared to be easily extendable, indicating good intermolecular extensibility. EA showed a more brittle nature because of enzymatic treatment that severed the molecular chains, hindering tight bonding. CA appeared thick, tight, and smooth, presumably via bonding by its highly branched side chains.

3.5. *Comparison of gelling properties of RGPs extracted by different methods*

Calcium-induced gels are favored in the food industry for their ability to rapidly form without requiring sucrose. These gels are bonded by “calcium bridges” between carboxyl groups and calcium ions, creating a gel network stronger than the hydrogen bonds and hydrophobic interactions observed in high sugar-containing gels (Donati et al., 2021). The gelling properties of RGPs were evaluated (Fig. 6A), revealing that HA pectin formed a weak gel with slight fluidity, whereas TP and EA RGP did not form gels. In contrast, AK and CA RGP produced hard gels. SEM was used to examine the microstructural differences of

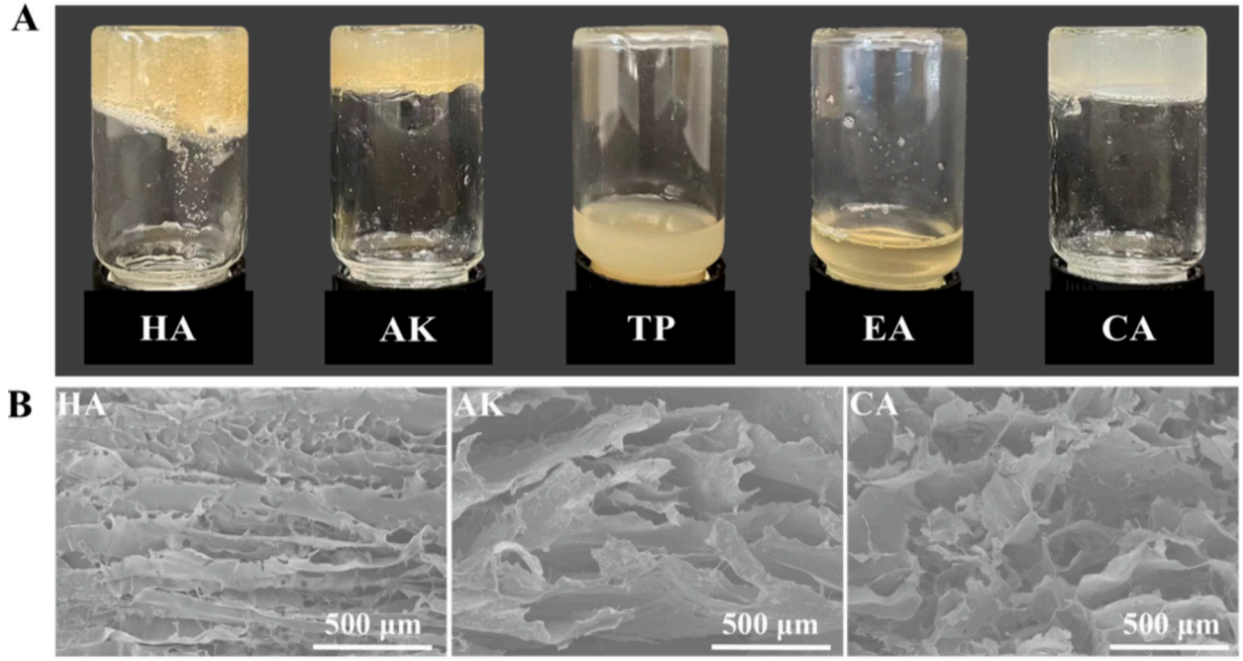

Fig. 6. (A) Macroscopic gelation status and (B) microstructure (80× magnification) of calcium-induced gels formed by different RGPs.

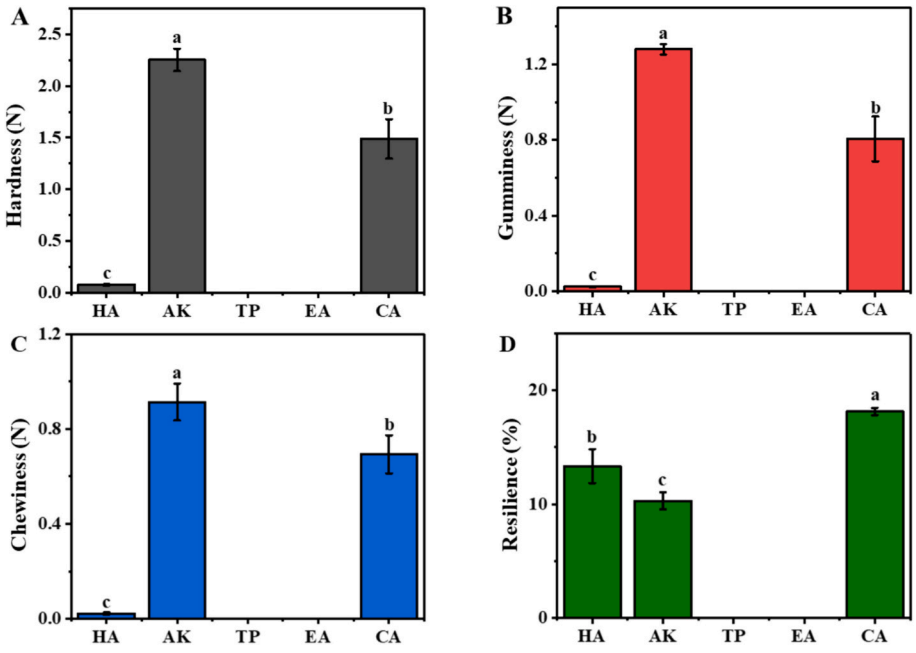

Fig. 7. Textural analysis of calcium-induced gels formed by different RGPs. (A) Hardness, (B) gumminess, (C) chewiness, and (D) resilience.

these gels (Fig. 6B); the results showed that HA gel had a thin lamellar structure with sparse fibrous networks. AK and CA gels displayed thicker walls; CA gel exhibited a more cross-linked network structure.

The texture properties of RGP gels (Fig. 7A-7D) demonstrated that AK and CA RGPs had superior physical properties, including hardness, gumminess, and chewiness, compared with HA pectin (AK gel > CA gel > HA gel). Regarding resilience, CA gel scored the highest at 18.38 %, with the following ranking: CA gel > HA gel > AK gel. The storage modulus (G′) and loss modulus (G″) of RGP gels were analyzed under a deformation of 0.1 % (Fig. 8). In HA pectin, AK, and CA RGP, G′ was higher than G″, suggesting successful gelation. HA gel's G′ and G″ values converged with increased frequency, indicating a weak and unstable gel network. TP and EA displayed higher G″ than G′ with observed crossover points between G′ and G″, consistent with gelation failure. However, both AK and CA gels exhibited high and stable G′ and G″ values, implying stability. The tan δ values of AK and CA gels were significantly lower (below 1) and more stable than those of HA, TP, and EA gels, indicating the superior elasticities of the former gels, in line with the higher G′ values. These findings underscore the potential of AK and CA RGP for applications in the food industry due to their ideal gelling properties.

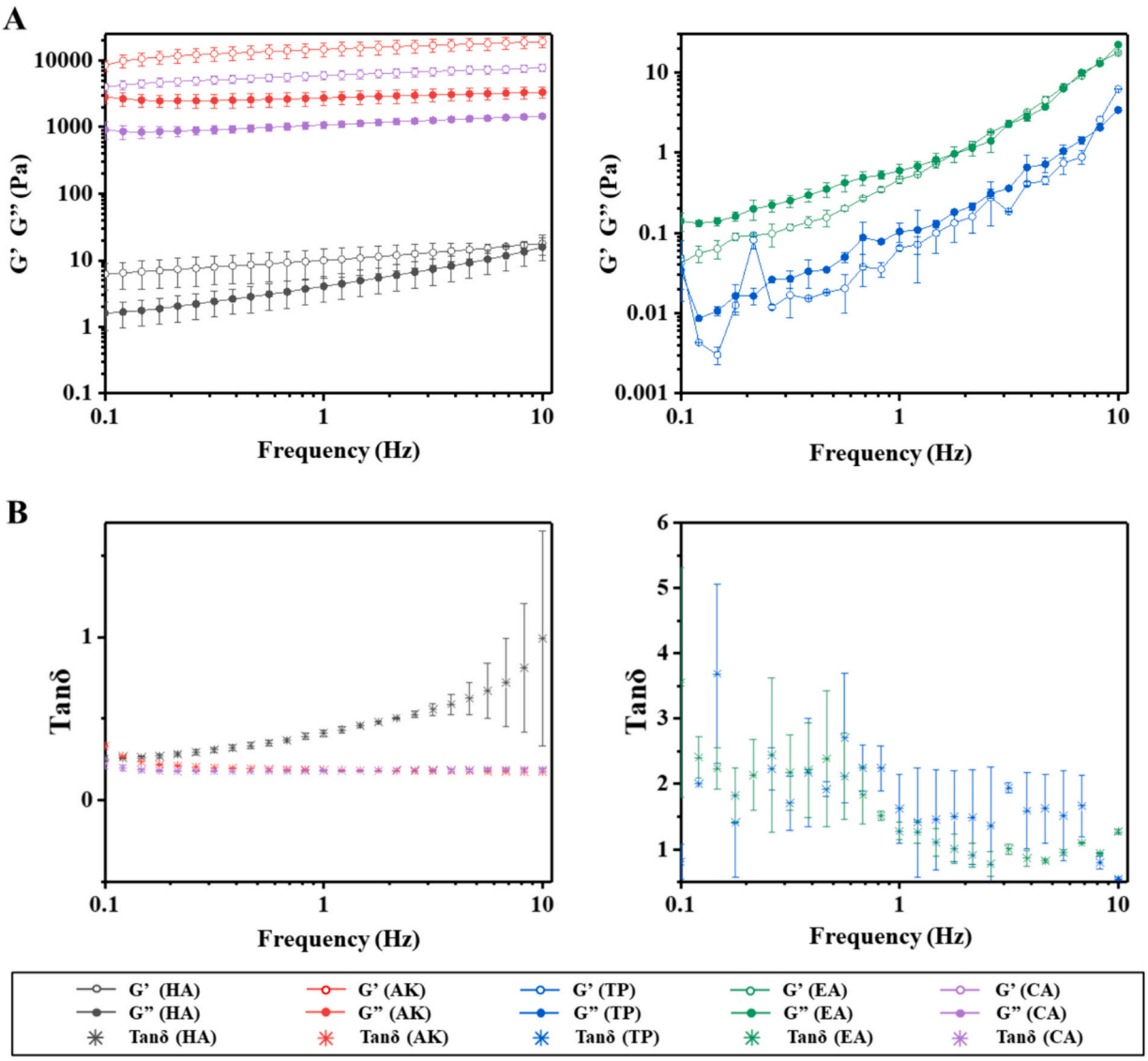

Fig. 8. The rheological properties of calcium-induced gels formed by different RGPs. (A) storage moduli (G′) and loss moduli (G″); (B) Tan δ.

3.6. Relationships between structural characteristics and gelling properties of RGPs extracted by different methods

Previous studies have demonstrated the significance of HG structural features, particularly the DE, in defining the gelling properties of pectin; the amount and exposure of carboxyl groups determine the binding sites for Ca^{2+} and affect the rheological characteristics of pectin gels (Fraeye et al., 2010). The neutral sugar chains in RG-I region act as structural stability factor that contributed to gelation by water-binding, entangling, intramolecular hydrophobic interactions (Mikshina et al., 2017; Zheng et al., 2020). HA pectin, characterized by the highest HG content and a DE slightly over 50 %, had the largest spatial dimensions (Dmax, Rg, and Rc) and thus a looser conformation than those of other pectins, associated with inferior gelling. TP RGP had a lower HG content and a higher DE than HA pectin, indicating that fewer carboxyl groups were available to form "calcium bridges." Also, the self-curved molecular structure of TP RGP inhibited carboxyl group exposure and thus reduced the number of Ca^{2+} binding sites; no gel formed (Fig. 9). Although the HG content and the DE of EA RGP suggested that this RGP should form a Ca^{2+}-induced hydrogel, the low molar mass was associated with long distances between molecules that could not be bridged by Ca^{2+}; again, no gel formed. The AK and CA extractions significantly increased the RG-I contents by destroying the HG regions, compromising the formation of Ca^{2+} hydrogels. However, the AK and CA RGPs (with abundant side chains) formed robust gel networks with optimal physical properties, emphasizing the contributions of RG-I regions to gelation. Compared with CA RGP and HA pectin, AK extraction preserved longer side chains that facilitated molecular entanglement, as evidenced by the smaller Dmax and Rg values, and thus a more compact conformation. Consequently, the AK gel had superior hardness, gumminess, and chewiness. Conversely, the highly branched structure and shorter side chains of CA RGP facilitated elastic intramolecular hydrophobic interactions, resulting in a more cross-linked gel. The CA gel thus exhibited the highest resilience of all RGP gels, suggesting that the CA gel would recover well after deformation.

4. Conclusion

This study focused on the extraction effect, structural characteristics, and gelling properties of RGP extracted by various methods. Among the four methods examined, CA yielded the highest output; AK and CA extractions surpassed TP and EA in terms of the RG-I proportion. The curved molecular conformations and reduced molar masses of TP and EA RGPs led to their gelation failure. AK preserved longer side chains,

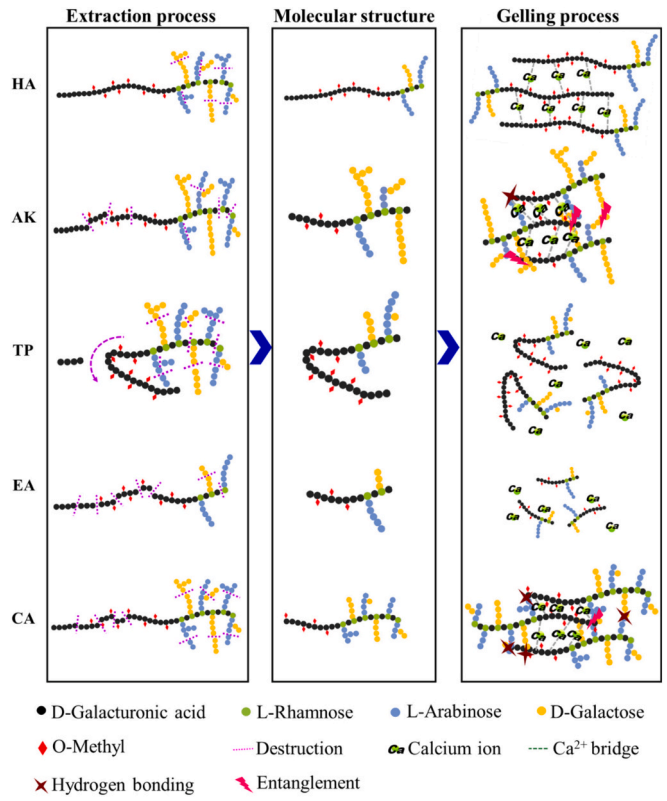

Fig. 9. Illustration of the relationships among extraction methods, structural characteristics, and gelling properties of RGPs.

reinforcing the gel network through side chain entanglements and producing a firm gel. Conversely, CA achieved a more branched structure with additional branching Rha and Ara preserved, which facilitated hydrogen bonding among molecules and resulted in a gel with higher resilience. The comparative insights provided by this study establish a foundation for research and development involving RGP-based gel materials with health-beneficial effects. Future research could focus on optimizing gel properties through the refinement of extraction process parameters.

CRediT authorship contribution statement

Xueping Wang: Writing – original draft, Methodology, Investigation. **Chengying Zhao:** Writing – original draft, Methodology, Investigation. **Jirong Wang:** Investigation. **Xingmiao Lu:** Validation. **Yuming Bao:** Investigation, Formal analysis. **Deli Zhang:** Writing – review & editing, Supervision, Project administration, Investigation, Conceptualization. **Jinkai Zheng:** Writing – review & editing, Supervision, Project administration, Funding acquisition, Formal analysis, Conceptualization.

Declaration of competing interest

The authors declare no competing financial interest.

Data availability

Data will be made available on request.

Acknowledgement

The authors would like to acknowledge the financial support provided by National Key R&D Program of China (No. 2023YFF1104005), National Natural Science Foundation of China (Nos. 32330084 and 32072181), Jiangsu Kolod Food Ingredients Co., Ltd., Central Public-interest Scientific Institution Basal Research Fund (Y2023PT21), Agricultural Science and Technology Innovation Program of Institute of Food Science and Technology, Chinese Academy of Agricultural Sciences (CAAS-ASTIP-G2022-IFST-06), and the Dutch research council NWO VENI grant (09150161910179 to D.Z). We also appreciate the National Elite Youth Program and Leading Scientist Program of Chinese Academy of Agricultural Sciences.

References

Alba, K., Laws, A. P., & Kontogiorgos, V. (2015). Isolation and characterization of acetylated LM-pectins extracted from okra pods. *Food Hydrocolloids, 43*, 726–735. https://doi.org/10.1016/j.foodhyd.2014.08.003

Chandel, V., Biswas, D., Roy, S., Vaidya, D., Verma, A., & Gupta, A. (2022). Current advancements in pectin: Extraction, properties and multifunctional applications. *Foods, 11*(17), 2683. https://doi.org/10.3390/foods11172683

Cheng, H. N., & Neiss, T. G. (2012). Solution NMR spectroscopy of food polysaccharides. *Polymer Reviews, 52*(2), 81–114. https://doi.org/10.1080/15583724.2012.668154

Chivero, P., Gohtani, S., Ikeda, S., & Nakamura, A. (2014). The structure of soy soluble polysaccharide in aqueous solution. *Food Hydrocolloids, 35*, 279–286. https://doi.org/10.1016/j.foodhyd.2013.06.006

Cui, J., Ren, W., Zhao, C., Gao, W., Tian, G., Bao, Y., Lian, Y., & Zheng, J. (2020). The structure-property relationships of acid- and alkali-extracted grapefruit peel pectins. *Carbohydrate Polymers, 229*, Article 115524. https://doi.org/10.1016/j.carbpol.2019.115524

Cui, J. F., Zhao, C. Y., Feng, L. P., Han, Y. H., Du, H. J., Xiao, H., & Zheng, J. K. (2021). Pectins from fruits: Relationships between extraction methods, structural characteristics, and functional properties. *Trends in Food Science & Technology, 110*, 39–54. https://doi.org/10.1016/j.tifs.2021.01.077

Cui, J. F., Zhao, C. Y., Zhao, S. J., Tian, G. F., Wang, F., Li, C. H., … Zheng, J. K. (2020). Alkali plus cellulase-extracted citrus pectins exhibit compact conformation and good fermentation properties. *Food Hydrocolloids, 108*, Article 106079. https://doi.org/10.1016/j.foodhyd.2020.106079

Donati, I., Benegas, J., & Paoletti, S. (2021). On the molecular mechanism of the calcium-induced gelation of pectate. Different steps in the binding of calcium ions by pectate. *Biomacromolecules, 22*(12), 5000–5019. https://doi.org/10.1021/acs.biomac.1c00958

Ferreira-Lazarte, A., Kachrimanidou, V., Villamiel, M., Rastall, R. A., & Moreno, F. J. (2018). Fermentation properties of pectins and enzymatic-modified pectins obtained from different renewable bioresources. *Carbohydrate Polymers, 199*, 482–491. https://doi.org/10.1016/j.carbpol.2018.07.041

Fraeye, I., Duvetter, T., Doungla, E., Van Loey, A., & Hendrickx, M. (2010). Fine-tuning the properties of pectin calcium gels by control of pectin fine structure, gel composition and environmental conditions. *Trends in Food Science & Technology, 21*(5), 219–228. https://doi.org/10.1016/j.tifs.2010.02.001

Hermansson, E., Schuster, E., Lindgren, L., Altskär, A., & Ström, A. (2016). Impact of solvent quality on the network strength and structure of alginate gels. *Carbohydrate Polymers, 144*, 289–296. https://doi.org/10.1016/j.carbpol.2016.02.069

Ho, C., Wang, Y. W., Liu, X. B., Zhou, Y. F., Pak, U., & Sun, L. (2023). Structural characterization of water-soluble polysaccharides isolated from leaves of *Hedera nepalensis*. *Chemical and Biological Technologies in Agriculture, 10*(1), 47. https://doi.org/10.1186/s40538-023-00427-2

Hou, Z. Q., Hu, X. X., Luan, L. Q., Yu, C. X., Wang, X. X., Chen, S. G., & Ye, X. Q. (2022). Prebiotic potential of RG-I pectic polysaccharides from *Citrus subcompressa* by novel extraction methods. *Food Hydrocolloids, 124*, Article 107213. https://doi.org/10.1016/j.foodhyd.2021.107213

Hu, W. W., Chen, S. G., Wu, D. M., Zhu, K., & Ye, X. Q. (2021). Physicochemical and macromolecule properties of RG-I enriched pectin from citrus wastes by manosonication extraction. *International Journal of Biological Macromolecules, 176*, 332–341. https://doi.org/10.1016/j.ijbiomac.2021.01.216

Khodaei, N., & Karboune, S. (2013). Extraction and structural characterisation of rhamnogalacturonan I-type pectic polysaccharides from potato cell wall. *Food Chemistry, 139*(1–4), 617–623. https://doi.org/10.1016/j.foodchem.2013.01.110

Li, F., Wei, Y. L., Liang, L., Huang, L. L., Yu, G. Y., & Li, Q. H. (2021). A novel low-molecular-mass pumpkin polysaccharide: Structural characterization, antioxidant activity, and hypoglycemic potential. *Carbohydrate Polymers, 251*, Article 117090. https://doi.org/10.1016/j.carbpol.2020.117090

Li, T., Senesi, A. J., & Lee, B. (2016). Small angle X-ray scattering for nanoparticle research. *Chemical Reviews, 116*(18), 11128–11180. https://doi.org/10.1021/acs.chemrev.5b00690

Lin, L. Y., Wang, P. P., Du, Z. Y., Wang, W. C., Cong, Q. F., Zheng, C. P., … Shao, C. H. (2016). Structural elucidation of a pectin from flowers of *Lonicera japonica* and its antipancreatic cancer activity. *International Journal of Biological Macromolecules, 88*, 130–137. https://doi.org/10.1016/j.ijbiomac.2016.03.025

Lu, X. M., Zhao, C. Y., Liu, D., Hu, M. X., Cui, J. F., Wang, F. Z., … Zheng, J. K. (2024). A novel prebiotic enzymatic hydrolysate of citrus pectin during juice processing. *Food Hydrocolloids, 146*, Article 109198. https://doi.org/10.1016/j.foodhyd.2023.109198

Maric, M., Grassino, A. N., Zhu, Z. Z., Barba, F. J., Brncic, M., & Brncic, S. R. (2018). An overview of the traditional and innovative approaches for pectin extraction from

plant food wastes and by-products: Ultrasound-, microwaves-, and enzyme-assisted extraction. *Trends in Food Science & Technology, 76*, 28–37. https://doi.org/10.1016/j.tifs.2018.03.022

Mikshina, P. V., Makshakova, O. N., Petrova, A. A., Gaifullina, I. Z., Idiyatullin, B. Z., Gorshkova, T. A., & Zuev, Y. F. (2017). Gelation of rhamnogalacturonan I is based on galactan side chain interaction and does not involve chemical modifications. *Carbohydrate Polymers, 171*, 143–151. https://doi.org/10.1016/j.carbpol.2017.05.013

Moslemi, M. (2021). Reviewing the recent advances in application of pectin for technical and health promotion purposes: From laboratory to market. *Carbohydrate Polymers, 254*, Article 117324. https://doi.org/10.1016/j.carbpol.2020.117324

Naqash, F., Masoodi, F. A., Rather, S. A., Wani, S. M., & Gani, A. (2017). Emerging concepts in the nutraceutical and functional properties of pectin-A review. *Carbohydrate Polymers, 168*, 227–239. https://doi.org/10.1016/j.carbpol.2017.03.058

Niu, H., Dou, Z. M., Hou, K. K., Wang, W. D., Chen, X. X., Chen, X. W., … Fu, X. (2023). A critical review of RG-I pectin: Sources, extraction methods, structure, and applications. *Critical Reviews in Food Science and Nutrition.*. https://doi.org/10.1080/10408398.2023.2204509

Pakhomov, N., & Baugh, J. A. (2021). The role of diet-derived short-chain fatty acids in regulating cardiac pressure overload. *American Journal of Physiology-Heart and Circulatory Physiology, 320*(2), H475–H486. https://doi.org/10.1152/ajpheart.00573.2020

Pappas, C. S., Malovikova, A., Hromadkova, Z., Tarantilis, P. A., Ebringerova, A., & Polissiou, M. G. (2004). Determination of the degree of esterification of pectinates with decyl and benzyl ester groups by diffuse reflectance infrared Fourier transform spectroscopy (DRIFTS) and curve-fitting deconvolution method. *Carbohydrate Polymers, 56*(4), 465–469. https://doi.org/10.1016/j.carbpol.2004.03.014

Saffer, E. M., Lackey, M. A., Griffin, D. M., Kishore, S., Tew, G. N., & Bhatia, S. R. (2014). SANS study of highly resilient poly(ethylene glycol) hydrogels. *Soft Matter, 10*(12), 1905–1916. https://doi.org/10.1039/c3sm52395k

Spinei, M., & Oroian, M. (2022). The influence of extraction conditions on the yield and physico-chemical parameters of pectin from grape pomace. *Polymers, 14*(7), 1378. https://doi.org/10.3390/polym14071378

Spinei, M., & Oroian, M. (2023). Structural, functional and physicochemical properties of pectin from grape pomace as affected by different extraction techniques. *International Journal of Biological Macromolecules, 224*, 739–753. https://doi.org/10.1016/j.ijbiomac.2022.10.162

Sun, L., Wu, D., Ning, X., Yang, G., Lin, Z. H., Tian, M. H., & Zhou, Y. F. (2015). α-Amylase-assisted extraction of polysaccharides from *Panax ginseng*. *International Journal of Biological Macromolecules, 75*, 152–157. https://doi.org/10.1016/j.ijbiomac.2015.01.025

Wang, J. R., Zhao, C. Y., Zhao, S. J., Lu, X. M., Ma, M. Y., & Zheng, J. K. (2023). Gelling properties of lysine-amidated citrus pectins: The key role of pH in both amidation and gelation. *Carbohydrate Polymers, 317*, Article 121087. https://doi.org/10.1016/j.carbpol.2023.121087

Wu, J., Shen, S., Gao, Q., Yu, C., Cheng, H., Pan, H., … Chen, J. (2023). RG-I domain matters to the in vitro fermentation characteristics of pectic polysaccharides recycled from citrus canning processing water. *Foods, 12*(5), 943. https://doi.org/10.3390/foods12050943

Yang, Z., Yang, H. J., & Yang, H. S. (2018). Effects of sucrose addition on the rheology and microstructure of κ-carrageenan gel. *Food Hydrocolloids, 75*, 164–173. https://doi.org/10.1016/j.foodhyd.2017.08.032

Yu, M., Xia, Y., Zhou, M., Guo, Y., Zheng, J., & Zhang, Y. (2021). Effects of different extraction methods on structural and physicochemical properties of pectins from finger citron pomace. *Carbohydrate Polymers, 258*, Article 117662. https://doi.org/10.1016/j.carbpol.2021.117662

Zhang, H., Chen, J. L., Li, J. H., Yan, L. F., Li, S., Ye, X. Q., … Chen, S. G. (2018). Extraction and characterization of RG-I enriched pectic polysaccharides from mandarin citrus peel. *Food Hydrocolloids, 79*, 579–586. https://doi.org/10.1016/j.foodhyd.2017.12.002

Zhang, M. Y., & Cai, J. (2023). Preparation of branched RG-I-rich pectin from red dragon fruit peel and the characterization of its probiotic properties. *Carbohydrate Polymers, 299*, Article 120144. https://doi.org/10.1016/j.carbpol.2022.120144

Zhao, J., Zhang, F. M., Liu, X. Y., Ange, K. S., Zhang, A. Q., Li, Q. H., & Linhardt, R. J. (2017). Isolation of a lectin binding rhamnogalacturonan-I containing pectic polysaccharide from pumpkin. *Carbohydrate Polymers, 163*, 330–336. https://doi.org/10.1016/j.carbpol.2017.01.067

Zheng, J. Q., Chen, J. L., Zhang, H., Wu, D. M., Ye, X. Q., Linardt, R. J., & Chen, S. G. (2020). Gelling mechanism of RG-I enriched citrus pectin: Role of arabinose side-chains in cation- and acid-induced gelation. *Food Hydrocolloids, 101*, Article 105536. https://doi.org/10.1016/j.foodhyd.2019.105536

Zhou, L. S., Huang, L. L., Yue, H., & Ding, K. (2018). Structure analysis of a heteropolysaccharide from fruits of *Lycium barbarum* L. and anti-angiogenic activity of its sulfated derivative. *International Journal of Biological Macromolecules, 108*, 47–55. https://doi.org/10.1016/j.ijbiomac.2017.11.111